Energy Cost Analysis of Membrane Distributed-Reflector Lasers for On-Chip Optical Interconnects

Takuo Hiratani, *Student Member, IEEE*, Takahiko Shindo, *Member, IEEE*, Kyohei Doi, Yuki Atsuji, Daisuke Inoue, Tomohiro Amemiya, *Member, IEEE*, Nobuhiko Nishiyama, *Senior Member, IEEE*, and Shigehisa Arai, *Fellow, IEEE*

***Abstract*—The power consumption of lateral-current-injection semiconductor membrane distributed-reflector lasers with a λ/4 shift region has been theoretically evaluated, in terms of their ultralow-power-consumption and high-speed modulation operations. This paper contains an investigation into the optimal structure of the membrane laser in terms of its energy cost, for use in on-chip optical interconnections. The total power consumption was evaluated, taking Joule heating into account by assuming the device resistance. It was found that the large Joule heating effect present in shorter cavities limits a reduction of their power consumption. As a result, an energy cost of 63 fJ/bit can be obtained for 10 Gb/s data transmission, while maintaining the necessary power output required for a cavity length of 12 μm. We have provided a guide for designing microcavity lasers in terms of their Joule heating power.**

***Index Terms*—DFB laser, DR laser, lateral current injection, membrane laser, optical interconnection, semiconductor laser.**

I. Introduction

THE performance of large-scale integrated circuits (LSIs) have been improved following the scaling law [1]. However, as the scaling advances, various problems including resistor-capacitor (RC) delay or Joule heating due to the skin effect in the electrical interconnections are limitting the improvement [2], [3]. Optical interconnection is expected as one of the candidates to solve these problems in future LSIs [4]–[6]. In the optical devices for such on-chip optical interconnection, ultralow-power-consumption operation and a small footprint, compared with the optical devices generally used for conventional optical fiber communications, are strongly required. The available power consumption (energy cost for data transport) for a light source in an on-chip optical interconnection except driving electronics is estimated to be 100 fJ/bit or less [7]. This simply implies that the bias current of the light source is limited to be less than 1 mA with assumptions of 10 Gb/s direct modulation and bias voltage of 1 V. As the light sources satisfying these requirements, microcavity lasers including vertical cavity surface-emitting lasers (VCSELs) [8]–[11] or microdisk lasers [12], [13] have been reported. These are promising devices for ultralow power consumption operation because of their strong optical confinement structures. Photonic crystal (PhC) lasers also have been studied as ultralow power consumption lasers [14], [15]. The electrically pumped PhC lasers have already been demonstrated [16]–[18], and the operating energy cost of 4.4 fJ/bit was achieved recently [19]. However, in the measurement, an avalanche photodiode, which needs much higher bias voltage as well as higher cosumption power than a pin photodiode, was used, and the measured bit error rate (BER) was 10^{-3} which was far from an error free opration required for an optical interconnect (BER $= 10^{-9}$ or the less). Moreover, too strong optical confinement into the PhC cavity will limit the design of adequate cavity length for low power consumption and high-speed modulation capability. The Joule heating is also expected to be a serious problem for these extremely small cavity lasers.

We have proposed and demonstrated semiconductor membrane lasers consisting of a thin semiconductor membrane core layer sandwiched by low-refractive-index cladding layers such as air or SiO_2. This large refractive index difference between them enhances the optical confinement in the active layer by a factor of approximately 3, and it contributes to drastic reduction of the threshold current in the membrane laser. Actually, such ultralow threshold operation was demonstrated under an optical pump with room-temperature continuous-wave (RT-CW) condition [20]–[22]. Since this enhancement of the optical confinement into the membrane structure also enhances an index-coupling coefficient of a grating structure and it becomes between that of PhC structure and conventional semiconductor DFB lasers, a possiblity of membrane DFB lasers with low power consumption operation as well as high-speed modulation capability was proposed. In order to realize electrical pumping of the membrane laser, we have introduced a lateral-current-injection (LCI) structure [23] formed by a two-step regrowth process because it is difficult to inject the current along the vertical direction owing to the upper and lower insulating cladding layers. Consequently, electrically pumped DFB lasers with a surface grating structure have been demonstrated [24], and a low threshold current of 3.8 mA was obtained by the benzocyclobutene (BCB) bonding process [25]. After that, a membrane laser with a 220 nm thick core layer was fabricated, and RT-CW

Manuscript received February 13, 2015; revised May 11, 2015 and June 20, 2015; accepted July 11, 2015. Date of publication July 14, 2015; date of current version September 1, 2015. This work was supported by the JSPS KAKENHI under Grants 24246061, 15H05763, 25709026, 21226010, and 25420321.

T. Hiratani, K. Doi, Y. Atsuji, D. Inoue, and N. Nishiyama are with the Department of Electrical and Electronic Engineering, Tokyo Institute of Technology, Tokyo 152-8552, Japan (e-mail: hiratani.t.aa@m.titech.ac.jp; doi.k.ac@m.titech.ac.jp; atsudi.y.aa@m.titech.ac.jp; inoue.d.ac@m.titech.ac.jp; n-nishi@pe.titech.ac.jp).

T. Shindo, T. Amemiya, and S. Arai are with the Quantum Nanoelectronics Research Center, Tokyo Institute of Technology, Tokyo 152-8552, Japan (e-mail: shindou.t.aa@m.titech.ac.jp; amemiya.t.ab@m.titech.ac.jp; arai@pe.titech.ac.jp).

Color versions of one or more of the figures in this paper are available online at http://ieeexplore.ieee.org.

Digital Object Identifier 10.1109/JSTQE.2015.2456334

1077-260X © 2015 IEEE. Personal use is permitted, but republication/redistribution requires IEEE permission.
See http://www.ieee.org/publications_standards/publications/rights/index.html for more information.

operation with a threshold current of 3.5 mA was performed by reducing the thickness of the BCB to achieve lower thermal resistance [26]. A membrane DFB laser comprised of a butt-jointed built-in (BJB) structure was recently fabricated [27], and a sub-mA threshold current operation was obtained for the first time. Further, a lateral current injection DFB laser on SiO_2/Si substrate by O_2-plasma-assisted direct bonding with threshold current of 0.9 mA and 25.8 Gb/s modulation operation also was demonstrated [28]. However, the energy cost of 171 fJ/bit is not enough for on-chip light sources. In a theoretical analysis of the LCI-membrane DFB laser, a design of low threshold current and high-speed (>10 Gb/s) direct modulation was reported for on-chip optical interconnections [29]. However, detail studies in the view point of energy cost have not been done yet.

In this paper, the optimal structure of the membrane laser is investigated in terms of its energy cost, for use in on-chip optical interconnections. Section II describes the method used for calculating the power consumption of DFB lasers with various index coupling coefficients, $\kappa_{\rm i}$. In Section III, a membrane laser with a distributed-reflector (DR) structure, which exhibits a high output efficiency from one side, is investigated in terms of required current for on-chip optical interconnection. In Section IV, the total power consumption of the LCI-membrane DR laser, for both low-power-consumption and high-speed operation, is estimated by assuming a series resistance. The results indicate that the total power consumption is limited by the Joule heating, with a reduction in cavity length. In Section V, the energy cost of a membrane DR laser is estimated.

II. Calculation Procedure for Power Consumption in LCI-Membrane DR Laser

For a light source in an on-chip optical interconnection, a certain light output power level depending on the transmission speed and receiver sensitivity is required. In this section, before estimating the total power consumption of the LCI- membrane DR laser, the calculation procedure of the total power consumption, which meets the requirements of the light output power and modulation speed for various index-coupling coefficients $\kappa_{\rm i}$, is provided. The index-coupling coefficient is expressd by $\kappa_{\rm i} = (A/2) \cdot (2\pi/\lambda_0) \cdot \Delta n$ [30]. The constant coefficient A is determined by the grating structure, λ_0 is the lasing wavelength and Δn is the difference of refractive index. Fig. 1 shows the flow chart of the procedure used in the calculation of the total power consumption in a DFB laser for a desired index-coupling coefficient. The total power consumption for various index-coupling coefficients can be obtained by repeating this procedure. First, for the given index-coupling coefficient $\kappa_{\rm i}$ of a DFB laser, the cavity length L dependences of the threshold current $I_{\rm th}$ and an external differential quantum efficiency for the front side $\eta_{\rm df}$ are calculated by using the coupled-wave-theory (CWT) [31] or transfer-matrix-method (TMM) [32]. The threshold current $I_{\rm th}$ and the external differential quantum efficiency $\eta_{\rm df}$ are expressed as in Eqs. (1)–(3) in refs. [33] and [34],

$$I_{\rm th} = \frac{eV_{\rm a}}{\eta_{\rm i}} \left\{ B \left(N_{\rm tr} e^{\frac{g_{\rm th}}{g_0}} \right)^2 + C \left(N_{\rm tr} e^{\frac{g_{\rm th}}{g_0}} \right)^3 \right\}, \quad (1)$$

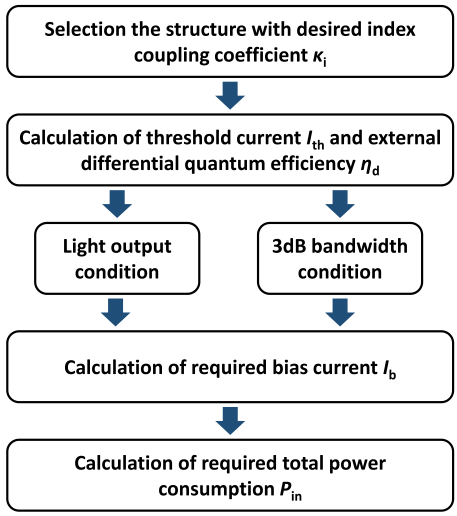

Fig. 1. Calculation procedure for total power consumption of LCI-membrane DFB laser for a desired index coupling coefficient.

$$\xi g_{\rm th} = \alpha_{\rm m} + \alpha_{\rm WG}, \quad (2)$$

$$\eta_{\rm df} = \eta_{\rm i} \frac{\alpha_{\rm m}}{\alpha_{\rm m} + \alpha_{\rm WG}} \frac{P_{\rm f}}{P_{\rm o}}, \quad (3)$$

where e is the unit of electron charge, $V_{\rm a}$ is the active region volume, $\eta_{\rm i}$ is the internal quantum efficiency, B is the bimolecular recombination coefficient, C is the Auger coefficient, $N_{\rm tr}$ is the transparent carrier density, g_0 is the gain coefficient, ξ is the optical confinement factor, $g_{\rm th}$ is threshold gain, $\alpha_{\rm m}$ is the mirror loss, $\alpha_{\rm WG}$ is the waveguide loss, and $P_{\rm f}/P_{\rm o}$ is the ratio of the output power to that on front side. Further, the bias currents $I_{\rm b}$ for the required light output and modulation speed are calculated by substituting the threshold current Ith and the external differential quantum efficiency $\eta_{\rm df}$ into the following equations, respectively,

$$P_{\rm f} = \frac{h\nu}{e} \eta_{\rm df} (I_{\rm b} - I_{\rm th}), \quad (4)$$

$$f_{\rm 3dB} \approx \frac{1.55}{2\pi} \sqrt{\frac{\xi G' \eta_{\rm i}}{eV_{\rm a}}} \sqrt{I_{\rm b} - I_{\rm th}}, \quad (5)$$

where h is the Planck's constant, ν is the optical frequency, $I_{\rm b}$ is the bias current, ξ is the optical confinement factor and G' is the differential gain per unit time. In this study, we ignored the self heating effect and dumping effect. Although the membrane structure has large thermal resistance, the operation current is relatively low due to ultra-low threshold current and the self-heating is smaller than 10 K at such bias condition [35]. For 10 Gb/s operation, the dumping effect is also small with an assumption of delay time of 15 ps [29]. This delay time includes carrier transport in optical confinement layer (∼1 ps), carrier capture time from the barrier layer to the quantum well layers, and RC product of LCI structure (< 1 ps). Furthermore, the required total power consumption for the required light output and modulation speed is calculated by substituting the required bias current $I_{\rm b}$ obtained above into

$$P_{\rm in} = \left(\frac{h\nu}{e} + RI_{\rm b} \right) I_{\rm b} = \frac{h\nu}{e} I_{\rm b} + RI_{\rm b}^2, \quad (6)$$

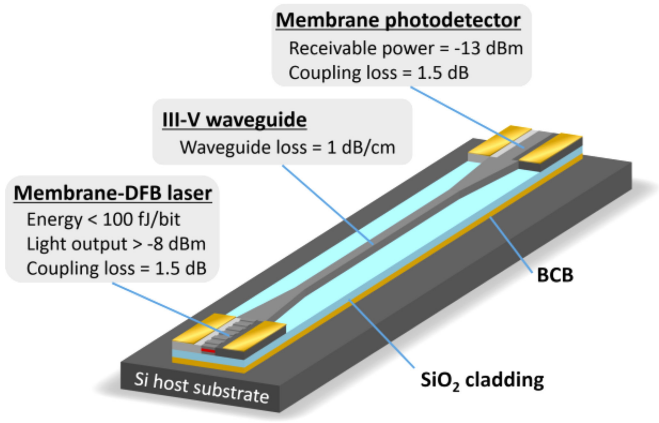

Fig. 2. Schematic diagram of a membrane-based photonic integrated circuit.

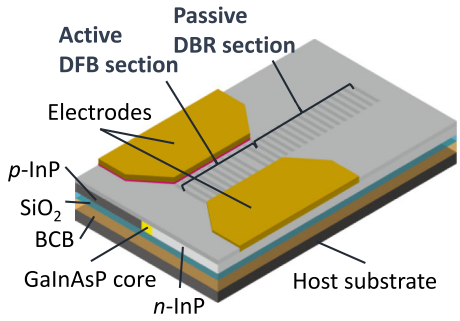

Fig. 3. Schematic diagram of the LCI-membrane DR laser with a surface grating structure.

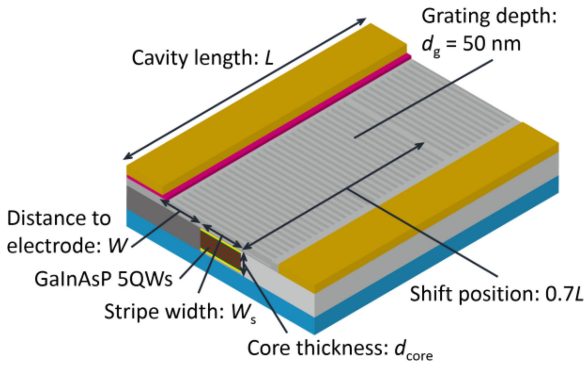

Fig. 4. Schematic structure of an LCI-membrane DR laser (DFB region) used for the calculation of the lasing characteristics.

where $h\nu/e$ is the turn-on voltage of the laser diode decided by energy gap and R is the device resistance. On the right-hand side of Eq. (6), the first term includes the input power for the light output, and the second term represents the power consumed in the resistance, namely, Joule heating power. Finally, the minimum total power consumption for the given index coupling coefficient κ_i is obtained from the cavity length dependence of the total power consumption, and the optimal cavity length for low-power-consumption operation with a given κ_i is determined. By applying the above procedure to the various index coupling coefficients, the index coupling coefficient κ_i (or cavity length L) dependence of the power consumption and the energy cost are obtained for the required light output or modulation speed. In order to obtain the total power consumption, which meets the both the required light output and modulation speed, it is required to plot the total power consumption under these two conditions and to select the one with the higher value. In this paper, we use this procedure to estimate the power consumption of membrane lasers.

III. Required Bias Current of LCI-Membrane Lasers for Ultralow-Power-Consumption Operation

We have proposed membrane photonic-integrated-circuits (PICs) including LCI-membrane lasers, III–V waveguides, and membrane photodetectors as shown in Fig. 2 as candidates for an in-plane photonic platform with ultralow power consumption [36]. The on-chip light sources has large advantages in terms of energy efficiency and energy proportionality [37]. As previously mentioned, the available consumption energy (energy cost for data transport) for a light source in an optical interconnect is estimated to be approximately 100 fJ/bit or less [7]. This implies that the available bias current of the light source is limited to less than 1 mA when a modulation speed of 10 Gb/s and driving voltage of 1 V are assumed. The output power of the light source is also important and is determined by the minimum receivable power of the photodetector and other losses. Here, we assume a minimum receivable power of –13 dBm (0.05 mW), which is usually used for a GaInAs p-i-n photodiode (PIN-PD) without any expensive limiting amplifier at 10 Gb/s transmission rate with a bit error rate (BER) of 10^{-9}. The link loss is assumed to be 5 dB, including coupling loss between the waveguide and the detector (1.5 dB), transmission loss in the membrane waveguide of the length of 2 cm (2 dB), and coupling loss between the waveguide and the laser (1.5 dB). We can reduce the coupling loss by introducing taper structure.Therefore, the required light output is estimated to be -8 dBm (0.16 mW) for 10 Gb/s transmission.

As a light source of the on-chip optical interconnection, we have proposed and demonstrated LCI-membrane DFB lasers with a surface grating structure. However, with only a simple DFB structure with uniform grating [29], the same amount of light output power is emitted from both sides. This implies that half of the light output power is unused. Therefore, we propose to use the distributed-reflector (DR) structure [38]–[40] into the LCI-membrane laser with a surface grating structure as shown in Fig. 3 in order to improve the power at one side. The LCI-membrane DR laser consists of a III–V waveguide, a DFB section, and a DBR section. The III–V waveguide with a GaInAsP core layer is assumed to be formed by the BJB waveguide [27].

The DFB section consists of an LCI-membrane structure with GaInAsP multiple quantum wells [29] as shown in Fig. 4. We additionally introduce a surface grating with a $\lambda/4$ phase-shift for the reduction of the threshold current by strong optical confinement along the longitudinal direction. The position of the $\lambda/4$ phase-shift region is set to $0.7L$ (L is the length of the DFB section.) from the boundary at the output side because the lower threshold current is obtained with higher external differential quantum efficiency under this condition. The DBR section with

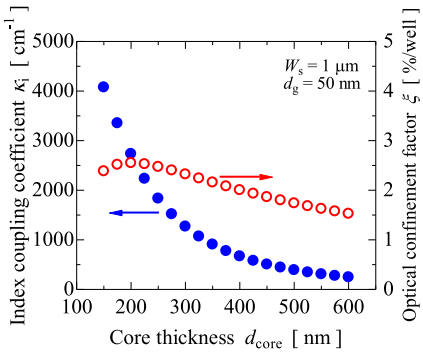

Fig. 5. Core thickness dependence of index coupling coefficient κ_i and optical confinement factor ξ.

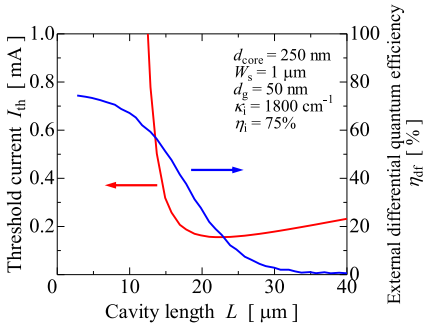

Fig. 6. Threshold current and external differential quantum efficiency as functions of the cavity length of the LCI-membrane DR laser with $d_{\rm core} = 250$ nm.

high reflectivity can realize high output efficiency from one side. In the calculation, the reflectivities of the DBR and the output end are assumed to be 99% and 0%, respectively.

First, we calculated the bias current satisfying the requirements for on-chip optical interconnection at a given index-coupling coefficient $\kappa_{\rm i}$ for a LCI-membrane DR laser with a surface grating structure. We adjusted $\kappa_{\rm i}$ by varying the thickness of the core layer $d_{\rm core}$ at a constant grating depth of $d_{\rm g} = 50$ nm, as shown in Fig. 5, assuming a stripe width of 1 μm. It was found that a thinner core layer leads to an increase in both the index-coupling coefficient and the optical confinement factor [41]. This implies that a thinner core structure of between 150–250 nm may be advantageous in terms of low-threshold current operation. In this paper, we used the TMM in order to calculate the threshold current and the external differential quantum efficiency, as the membrane structure has large refractive-index difference. The index-coupling coefficient was calculated by assuming the presence of rectangular shaped grooves with a width of half the period of the grating, and was determined by the core layer thickness, as shown in Fig. 5.

The threshold current and external differential quantum efficiency, as a function of the cavity length of a LCI-membrane DR laser with a core thickness of 250 nm, is shown in Fig. 6. In this study, we called active DFB section length to the cavity length. The threshold current is calculated by substituting into Eq. (1) and (2) the internal quantum efficiency $\eta_{\rm i}$ of 75% and the waveguide loss $\alpha_{\rm WG}$ of 42 cm^{-1}, which were obtained in our previous work [42]. The other parameters used

TABLE I
PARAMETERS FOR CALCULATION OF THRESHOLD CURRENT AND EXTERNAL QUANTUM EFFICIENCY [34], [43]

Parameters	Value
Bimoleculor recombination coefficient B	1.6×10^{-10} cm^3/s
Auger coefficient C	5×10^{-29} cm^6/s
Transparent carrier density $N_{\rm tr}$	1.5×10^{18} cm^{-3}
Gain coefficient g_0	1500 cm^{-1}

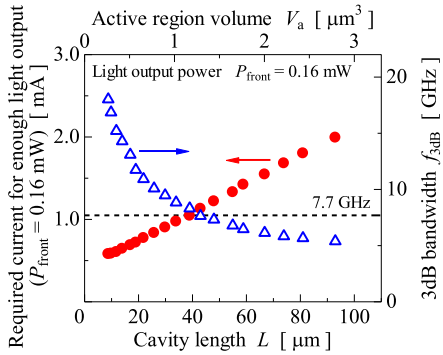

Fig. 7. Cavity length dependences of the bias current required for the light output ($P_{\rm front} = 0.16$ mW) and 3 dB bandwidth of the LCI-membrane DR laser.

in this calculation, which are typical values for GaInAsP/InP strain-compensated MQWs [34], [43], are listed in Table I. It can be seen that a threshold current reduces with shortening the cavity length and takes the minimum value of 155 μA at 22 μm and then drastically increases because of an increase of the mirror loss. At the cavity length of 22 μm, an external differential quantum efficiency at the front side $\eta_{\rm df}$ of 17% can be obtained.

Furthermore, the required bias current was calculated for the ultralow-power-consumption operation with a high-speed direct modulation of the LCI-membrane DR laser. As mentioned before, a light output power of 0.16 mW at a modulation speed of 10 Gb/s is required by the light source of the on-chip optical interconnection. We assume that a 3 dB bandwidth $f_{\rm 3dB}$ of 7.7 GHz is required for a bit rate of 10 Gb/s, as the bit rate is 1.3 times higher than the $f_{\rm 3dB}$ in the non-return-to-zero (NRZ) signals [18], [19], [44]. The bitrate of 10 Gb/s is our first target for on-chip optical interconnection in the future LSI because the bitrate is moving up as growth of the clock frequency. Eqs. (4) and (5) were used in order to calculate $f_{\rm 3dB}$ and the light output power $P_{\rm front}$.

The bias current for the required light output power ($P_{\rm front} = 0.16$ mW) and $f_{\rm 3dB}$ at the given bias current as functions of the cavity length are shown in Fig. 7. In this calculation, the cavity length is chosen at the point of the minimum required current for the given $\kappa_{\rm i}$. The required current tends to decrease as the cavity length decreases, while $f_{\rm 3dB}$ also tends to increase. Therefore, the shorter cavity length is advantageous for lower bias current operation as well as faster direct modulation, and $f_{\rm 3dB}$ of more than 7.7 GHz is obtained when the cavity length is less than 40 μm. The reason for the increase in $f_{\rm 3dB}$ with regard to the shorter cavity length is that the modulation speed

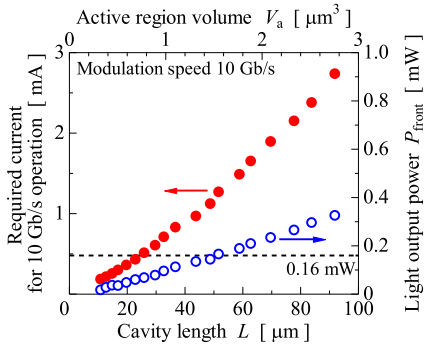

Fig. 8. Cavity length dependences of the bias current required for 10 Gb/s operation and light output power on the front side of the LCI-membrane DR laser.

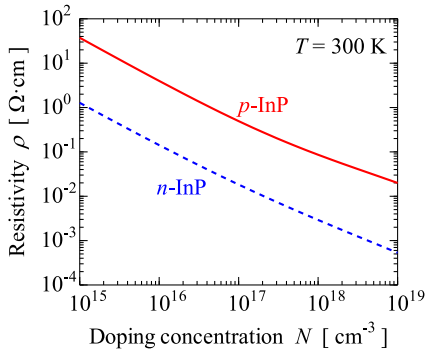

Fig. 9. Resistivities of p-InP and n-InP as a function of doping concentration plotted after experimental fitting [45].

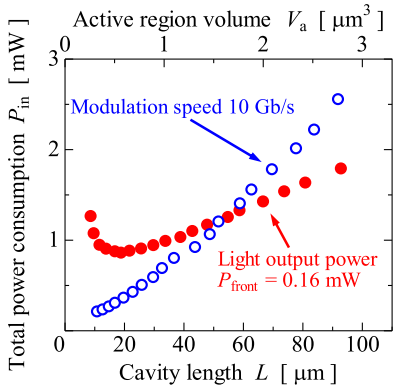

Fig. 10. Cavity length dependence of total power consumption for required light output power (0.16 mW) and that for 10 Gb/s operation.

strongly depends on the active region volume V_a rather than on the square root of the difference between the bias current and the threshold current $(I_b - I_{th})^{1/2}$ as in Eq. (5). This implies that the requirements for both light output power and modulation speed can be satisfied when the cavity length is less than 40 μm.

On the other hand, the required current for 10 Gb/s operation and light output power P_{front} at each bias current are calculated as functions of the cavity length as shown in Fig. 8. In this calculation, the cavity length is also chosen at the point of minimum bias current for a given coupling coefficient κ_i. Both the bias current and the light output power tend to decrease as the cavity length decreases. Light output power P_{front} of more than 0.16 mW can be obtained when the cavity length is more than 40 μm. This implies that the requirements for both the light output power and modulation speed are satisfied with a cavity length of more than 40 μm, and the bias current is limited to the 3 dB bandwidth in this region. In the case of excluding the device resistance, these results show that it is important to realize a shorter cavity for ultralow-power-consumption operation.

Although some data points are fluctuated, these are caused from the rough resolution of the cavity length (approximately 1 μm) for TMM calculation. Further, the optimum cavity length in Fig. 7 is slightly differenct from that in Fig. 8, because the index coupling coefficient is also different for each cavity length.

IV. Power Consumption and Joule Heating

As discussed in the previous section III, a shorter cavity length is apparently advantageous for ultralow-power-consumption operation and high-speed modulation. However, it is expected that the shorter cavity structure induces higher series resistance particularly in the LCI-membrane DR lasers, which have a very thin p-InP layer and smaller cross section of the current injection path when compared with the conventional vertical injection type lasers. We have estimated the total power consumption and Joule heating power of the LCI-membrane DR lasers by using the device resistance because of the concern that Joule heating constitutes a limiting factor of the ultralow-power-consumption operation. In general, the resistivity ρ of the semiconductors is expressed as

$$\rho = \frac{1}{eN\mu}, \tag{7}$$

where N is the doping concentration and μ is the mobility. We have used the experimental fitting as the mobility of InP dependence on the doping concentration [45]. By using this mobility, the resistivities of p-InP and n-InP were calculated as shown in Fig. 9. It is shown that the resistivity of p-InP is one order of magnitude higher than that of n-InP; therefore, we assumed the resistance of the p-InP cladding layer as the device resistance by ignoring the resistance of the n-InP cladding and active region. We also ignored the contact resistance of p side and n side by assuming the ideal contact resistance of approximately 10^{-6} Ω·cm^2 [46], [47]. The resistivity of the p-InP cladding is assumed to be $\rho_{p\text{-InP}} = 0.086\ \Omega \cdot \mathrm{cm}$ at a doping concentration of $N_A = 1 \times 10^{18}\mathrm{cm}^{-3}$ from the result of Fig. 9. The resistance of the p-InP cladding region $R_{p\text{-InP}}$ is expressed as

$$R_{p\text{-InP}} = \rho_{p\text{-InP}} \frac{W}{d_{\mathrm{core}} L}, \tag{8}$$

where W is the distance between the active region and the p side metal contact. A distance W of 3 μm was assumed for the power consumption calculation. The total power consumption P_{in} can be obtained by Eq. (6).

Fig. 10 shows the cavity length dependence of the total power consumption for the light output of 0.16 mW and that for 10 Gb/s operation. In order to satisfy both the requirements, we need to adopt a higher value of the total power consumption

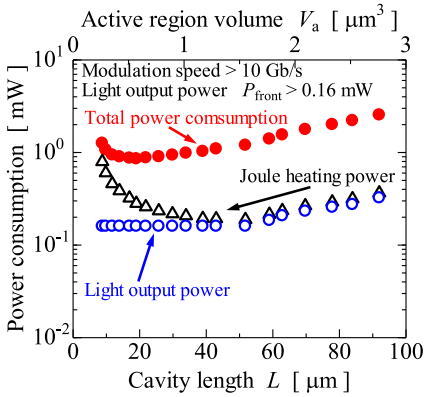

Fig. 11. Cavity length dependence of the total power consumption and Joule heating power required for the light output power (0.16 mW) and 10 Gb/s operation.

required for the light output of 0.16 mW (painted circles) and that for 10 Gb/s operation (open circles).

Fig. 11 shows the required total power consumption as well as Joule heating power and light output power as functions of the cavity length. As can be observed, the total power consumption decreased with a decrease in the cavity length to $L = 20$ μm; however, it tends to increase when $L < 20$ μm because the Joule heating power increases with an increase in the device resistance. In this case, the total power consumption takes the minimum value at $L = 19$ μm. Moreover, the Joule heating power accounts for 63% of the total power consumption at $L = 9$ μm; therefore Joule heating is a serious problem for ultralow-power-consumption and high-speed modulation operation of extremely low threshold semiconductor lasers particularly for on-chip interconnection.

In order to reduce the ratio of the Joule heating power to the total power consumption, an effective technique is to reduce the resistance of the *p*-InP cladding region $R_{p\text{-InP}}$. From Eq. (8), we observed that a reduction of the resistivity $\rho_{p\text{-InP}}$ and the electrode distance W is required, as d_{core} is used to determine the index-coupling coefficient κ_{i}, and L is optimized at a given κ_{i} in order to minimize the total power consumption. Optical loss must be considered as part of a discussion on resistivity $\rho_{p\text{-InP}}$, and electrode distance W. First, an increase in doping concentration causes not only a decrease in the resistivity, as shown in Fig. 9, but it also leads to an increased optical loss, as the *p*-InP has a relatively large absorption coefficient of 20 cm^{-1} for $N_A = 1 \times 10^{18}\text{cm}^{-3}$ [48]. Second, a short electrode distance also leads to an increased optical loss due to a large overlap in the optical mode field, as shown in Fig. 12. The absorption coefficients of Au and GaInAs are assumed to be 798000 and 5000 cm^{-1}, respectively. There also exists a trade-off between the resistance and the optical absorption loss of the mode. In order to estimate the effect of high doping and a short electrode distance, we evaluated the power consumption as a function of *p*-electrode distance. The dependence of the total power consumption on *p*-electrode distance is shown in Fig. 13, for $N_A = 1 \times 10^{18}\text{cm}^{-3}$ and $N_A = 4 \times 10^{18}\text{cm}^{-3}$, for a chosen core thickness of $d_{\text{core}} = 150$ nm. These doping concentration was chosen as the value of small affection to quantum well by

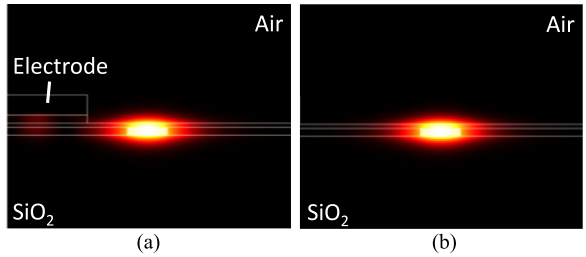

Fig. 12. Cross sectional mode profile of membrane laser at *p*-electrode distance of (a) 0.5 μm and (b) 1.5 μm.

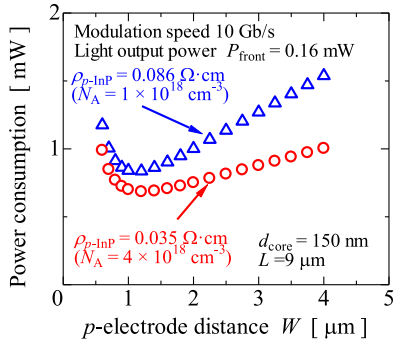

Fig. 13. *p*-electrode distance dependence of the total power consumption for $N_A = 1 \times 10^{18}\text{cm}^{-3}$ and $N_A = 4 \times 10^{18}\text{cm}^{-3}$.

p-type (Zn) dopant diffusion. A minimum power consumption of 0.68 mW was obtained at a *p*-electrode distance of 1.2 μm and a cavity length of 9 μm, with a doping concentration of $N_A = 4 \times 10^{18}\text{cm}^{-3}$. This result highlights two points of interest. One that high levels of doping are effective in cases with a longer electrode distance, and the increase of absorption in *p*-InP is small compared to the reduction in resistivity. The other point is that there exists an optimal electrode distance. When the electrode distance is less than 1.2 μm, the power consumption increases, because of an increase in the threshold current caused by the large optical loss at an electrode. On the other hand when the distance is more than 1.2 μm, the power consumption also increases due to an increase in resistance. This result also shows the tolerance of electrode distance. The average misalignment of our photolithography technique is approximately 0.5 μm. Therefore, the power co nsumption increase of 24% can be estimated from Fig. 13.

Fig. 14 shows the power consumption at the condition of $N_A = 4 \times 10^{18}\text{cm}^{-3}$ and electrode distance of 1.2 μm. Over the entire cavity length, the Joule heating power is drastically reduced when compared with the case of adopting $\rho_{p\text{-InP}} = 0.086\ \Omega \cdot \text{cm}$. The reduction in the *p*-InP cladding region resistivity $\rho_{p\text{-InP}}$ enables to suppress the Joule heating power to 24% of the total power consumption at the cavity length of 9 μm.

Fig. 15 summarizes the power conversion efficiency $P_{\text{o}}/P_{\text{in}}$ and the Joule heating ratio $P_{\text{Joule}}/P_{\text{in}}$ for $\rho_{p\text{-InP}} = 0.086\ \Omega \cdot \text{cm}$ and 0.035 Ω·cm. The Joule heating is totally reduced to less than 40% by a low resistivity $\rho_{p\text{-InP}} = 0.035\ \Omega \cdot \text{cm}$ when compared with high resistivity ($\rho_{p\text{-InP}} = 0.086\ \Omega \cdot \text{cm}$). Moreover, this reduction of the Joule heating power improves the power conversion efficiency and suppresses

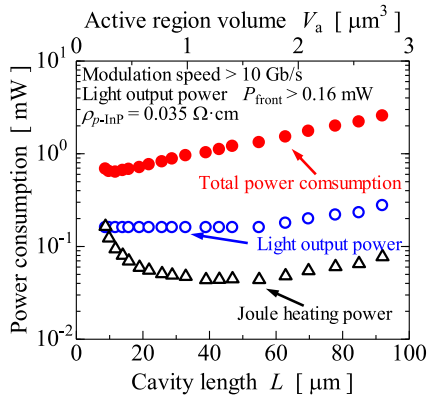

Fig. 14. Cavity length dependence of the total power consumption and Joule heating power required for the light output power (0.16 mW) and 10 Gb/s operation for the case of $\rho_{p\text{-InP}} = 0.035\ \Omega \cdot \mathrm{cm}$ and electrode distance of 1.2 μm.

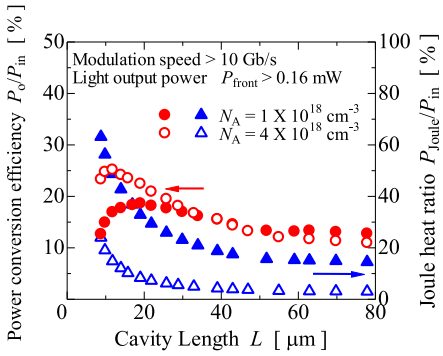

Fig. 15. Power conversion efficiency and Joule heating ratio of an LCI-membrane DR laser as functions of the cavity length.

the drastic decrease in the power conversion efficiency with regard to a shorter cavity length. In this figure, the power conversion efficiency of 25% is expected, and this value is realizable for InP material [49]. As a result, the reduction in the p-InP cladding region resistivity $\rho_{p\text{-InP}}$ is effective for microcavity lasers in order to reduce the Joule heating, which limits the ultralow-power-consumption operation.

V. Energy Cost Estimation

Finally, we have considered the energy cost for data transport (pulse energy), which is required energy for 1 bit data transport and expressed as

$$\text{Energy cost [J/bit]} = \frac{\text{Total power consumption [W]}}{\text{Bit rate [bit/s]}}. \quad (9)$$

This is the definition for ultralow-power-consumption and high-speed modulation operation. The calculated energy cost for 10 Gb/s data transport is shown in Fig. 16. As previously mentioned, the available power consumption for a light source in an on-chip optical interconnection is 100 fJ/bit or less. For a cavity length of less than 40 μm, the membrane DR laser is expected to achieve energy cost of less than 100 fJ/bit. For the 10 Gb/s direct modulation operation, it is appropriate to choose the cavity length of 12 μm (active region volume of 0.4 μm^3

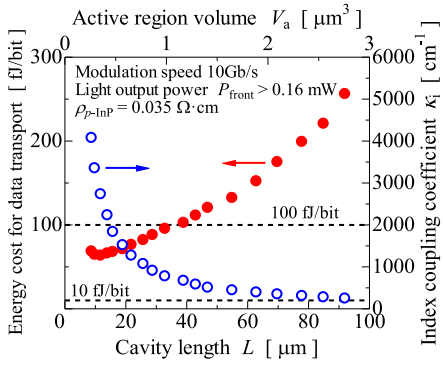

Fig. 16. Energy cost for 10 Gb/s data transport and index coupling coefficient of an LCI-membrane DR laser as functions of the cavity length.

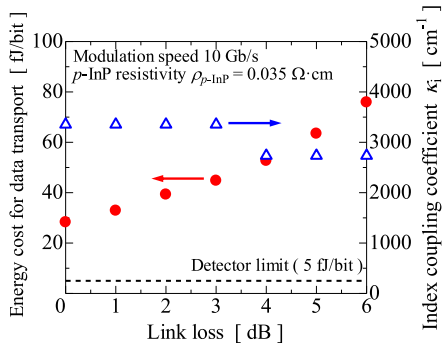

Fig. 17. Minimum energy cost at 10 Gb/s operation and index-coupling coefficient of an LCI-membrane DR laser as functions of the link loss.

and index-coupling coefficient κ_i of 2700 cm^{-1}), where the minimum energy cost of 63 fJ/bit can be obtained. For the cavity length of less than 12 μm, although the lower threshold current is obtained with high index-coupling coefficient grating, the total power consumption increases owing to the Joule heating. It is expected that further reduction in the resistivity of p-InP by higher doping concentration or reduction of electrode distance reduces the Joule heating in the shorter cavity, and a shorter cavity with higher index coupling coefficient κ_i is required for obtaining a minimum energy cost.

The recent requirement of energy cost for the light sources of an on-chip optical interconnection is approaching to less than 10 fJ/bit (predicted value in 2020) [7]. Therefore, as can be observed in Fig. 16, further reduction in the energy cost is required in the LCI-membrane DR laser. As one of methods to reduce the energy cost, we have considered the reduction in the required output power. This implies reduction in the minimum receivable power of the photodetector and link loss. The former is considered constant in this paper, because it is determined by the performance of the photodetector. We have mainly considered the latter. Fig. 17 shows that the energy cost at the 10 Gb/s direct modulation operation depends on the link loss. The minimum energy cost for each link loss is chosen. The detector limit is 5 fJ/bit because of the assumption that the minimum receivable power of detector is 0.05 mW (−13 dBm) in the 10 Gb/s operation. The energy cost tends to decrease as the link loss decreases. For the realization of lower link loss, the

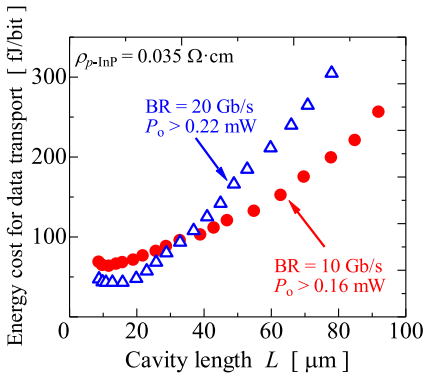

Fig. 18. Energy cost at 10, 20 Gb/s operation.

waveguide loss and coupling losses between the waveguide and the laser or detector should be reduced. In order to reduce the coupling loss, the introduction of taper structure is effective. It is also shown that a shorter cavity length with higher index coupling coefficient κ_i is suitable for the lower link loss structure. This implies that the low required bias current owing to the reduction in the required output power reduces the Joule heating. In the case of a link loss of 0 dB, an energy cost of 28 fJ/bit is obtained; this is the minimum energy cost of this structure for the 10 Gb/s operation. In order to obtain an energy cost of less than 10 fJ/bit, a smaller minimum receivable power of the photodetector with low power consumption of the detector itself should be assumed.

We also calculated the energy cost when using a bit rate of 20 Gb/s. The energy costs obtained using both 10 and 20 Gb/s operations are shown in Fig. 18. In these calculations, the required light output power is set to $2^{1/2} \times 0.16 = 0.22$ mW. This relation comes from the signal-to-noise ratio (SNR) for the p-i-n photodiode required in order to obtain the same BER as the 10 Gb/s operation [50]. The lowest energy cost obtained using the 20 Gb/s data transmission was of 43 fJ/bit, corresponding to a cavity length of 16 μm. This result indicates that a 20 Gb/s operation is more suitable for use in shorter cavity lasers (less than 30 μm in length), compared to a 10 Gb/s operation. The 10 Gb/s operation exhibited a large margin in its bias current because its power consumption was limited by the required light output power.

VI. Conclusion

We conducted theoretical investigations on the low-power consumption and high-speed direct modulation capabilities of an LCI-membrane DR laser for use in on-chip optical interconnections. A comparison was made with conventional LCI-membrane DFB lasers, in order to improve on their power conversion efficiency and these results indicate that the Joule heating power in the p-InP cladding region limits the ultralow-power-consumption operation in a shorter cavity. This is the common problem of ultra-small cavity laser to be solved.

First, the required bias current, obtained using both a 10 Gb/s direct modulation operation and a light output of 0.16 mW, was estimated. It was found that the bias current was limited by the light output required by a shorter cavity ($L < 50$ μm), and the modulation speed in a longer cavity ($L > 50$ μm). It was also shown that a short cavity with a high index coupling coefficient, κ_i, is advantageous in a low bias current operation.

Second, the total power consumption was calculated using the resistance of the p-InP cladding region. The Joule heating becomes a dominant effect in the shorter cavity region; although it can be reduced using a heavily doped p-InP cladding region and shorter electrode distance, which results in an improved power conversion efficiency.

Finally, we estimated the energy cost for 10 Gb/s data transport. It was found that an energy cost of less than 100 fJ/bit can be obtained using a cavity length of less than 40 μm, and the minimum value for the energy cost of a 10 Gb/s direct modulation operation was 63 fJ/bit using a cavity length of 12 μm. This indicates that the increased Joule heating in the shorter cavity limits the ultralow-power-consumption operation of the LCI-membrane DR lasers. It is also effective in reducing the link loss, an important factor in realizing low energy cost.

These results are significant for future membrane laser design, and they indicated that the membrane DR laser can realize not only low energy operation for on-chip optical interconnection but also various advantages including in-plane integration and controllability of light output compared with the alternatives, such as VCSELs, micro-disk lasers, PhC lasers, or off-chip lasers.

Acknowledgment

The authors would like to thank Professors S. Akiba, T. Mizumoto, M. Asada, Y. Miyamoto, and Associate Professor M. Watanabe of the Tokyo Institute of Technology for their fruitful discussions.

References

[1] R. H. Dennard, F. H. Gaensslen, V. L. Rideout, E. Bassous, and A. R. LeBlanc, "Design of ion-implanted MOSFET's with very small physical dimensions," *IEEE J. Solid-State Circuits*, vol. 9, no. 5, pp. 256–268, Oct. 1974.

[2] P. Kapur, J. P. McVittie, and K. C. Saraswat, "Technology and reliability constrained future copper interconnects—Part I: Resistance modeling," *Trans. Electron. Devices*, vol. 49, no. 4, pp. 590–597, Apr. 2002.

[3] P. Kapur, G. Chandra, J. P. McVittie, and K. C. Saraswat, "Technology and reliability constrained future copper interconnects—Part II: Performance implications," *Trans. Electron. Devices*, vol. 49, no. 4, pp. 598–604, Apr. 2002.

[4] D. A. B. Miller, "Rationale and challenges for optical interconnects to electronic chips," *Proc. IEEE*, vol. 88, no. 6, pp. 728–749, June 2000.

[5] G. Chen *et al.*, "Prediction of CMOS compatible on-chip optical interconnect," *Integr. VLSI J.*, vol. 40, no. 4, pp. 434–446, Oct. 2006.

[6] K. Ohashi *et al.*, "On-chip optical interconnect," *Proc. IEEE*, vol. 97, no. 7, pp. 1186–1198, Jul. 2009.

[7] D. A. B. Miller, "Device requirements of optical interconnects to silicon chips," *Proc. IEEE*, vol. 97, no. 7, pp. 1166–1185, Jul. 2009.

[8] P. Moser *et al.*, "81 fJ/bit energy-to-data ratio of 850 nm vertical-cavity surface emitting lasers for optical interconnects," *Appl. Phys. Lett*, vol. 98, no. 23, pp. 231106-1–231106-3, Jun. 2011.

[9] S. Imai *et al.*, "Recorded low power dissipation in highly reliable 1060-nm VCSELs for 'Green' optical interconnection," *IEEE J. Sel. Topics Quantum Electron.*, vol. 17, no. 6, pp. 1614–1620, Nov. 2011.

[10] A. Kasukawa, "VCSEL technology for green optical interconnects," *IEEE Photon. J.*, vol. 4 no. 2, pp. 642–646, Apr. 2012.

[11] M. P. Tan, A. M. Kasten, J. D. Sulkin, and K. D. Choquette, "Planar photonic crystal vertical-cavity surface-emitting lasers," *IEEE J. Sel. Topics Quantum Electron.*, vol. 19, no. 4, art. no. 4900107, Jul./Aug. 2013.

[12] M. Fujita, R. Ushigome, and T. Baba, "Continuous wave lasing in GaInAsP microdisk injection laser with threshold current of 40μA," *Electron. Lett.*, vol. 36, no. 9, pp. 790–791, Apr. 2000.

[13] J. V. Campenhout *et al.*, "Electrically pumped InP-based microdisk lasers integrated with nanophotonic silicon-on-insulator waveguide circuit," *Opt. Exp.*, vol. 15, no. 11, pp. 6744–6749, May 2007.

[14] S. Matsuo *et al.*, "High-speed ultracompact buried heterostructure photonic-crystal laser with 13 fj of energy consumed per bit transmitted," *Nature Photon.*, vol. 4, no. 9, pp. 648–654, Sep. 2010.

[15] S. Matsuo *et al.*, "20-Gbit/s directly modulated photonic crystal nanocavity laser with ultra-low power consumption," *Opt. Exp.*, vol. 19, no. 3, pp. 2242–2250, Jan. 2011.

[16] B. Ellis *et al.*, "Ultralow-threshold electrically pumped quantum-dot photonic-crystal nanocavity laser," *Nature Photon.*, vol. 5, no. 5, pp. 297–300, May 2011.

[17] S. Matsuo *et al.*, "Room-temperature continuous-wave operation of lateral current injection wavelength-scale embedded active-region photonic-crystal laser," *Opt. Exp.*, vol. 20, no. 4, pp. 3773–9780, Feb. 2012.

[18] S. Matsuo *et al.*, "Ultralow operating energy electrically driven photonic crystal lasers," *IEEE J. Sel. Topics Quantum Electron.*, vol. 19, no. 4, art. no. 4900311, Jul./Aug. 2013.

[19] K. Takeda *et al.*, "Few-fJ/bit data transmissions using directly modulated lambda-scale embedded active region photonic-crystal lasers," *Nature Photon.*, vol. 7, no. 7, pp. 569–575, Jul. 2013.

[20] T. Okamoto *et al.*,"Optically pumped membrane BH-DFB lasers for low-threshold and single-mode operation," *IEEE J. Sel. Topics Quantum Electron.*, vol. 9, no. 5, pp. 1361–1366, Sep./Oct. 2003.

[21] S. Sakamoto *et al.*, "Strongly index-coupled membrane BH-DFB lasers with surface corrugation grating," *IEEE J. Sel. Topics Quantum Electron.*, vol. 13, no. 5, pp. 1135–1141, Sep./Oct. 2007.

[22] S. Sakamoto *et al.*, "85 °C continuous-wave operation of GaInAsP/InP-membrane buried heterostructure distributed feedback lasers with polymer cladding layer," *Jpn. J. Appl. Phys.*, vol. 46, no. 47, pp. L1155–L1157, Nov. 2007.

[23] K. Oe, Y. Noguchi, and C. Caneau, "GaInAsP lateral current injection lasers on semi-insulating substrates," *IEEE Photon. Technol. Lett.*, vol. 6, no. 4, pp. 479–481, Apr. 1994.

[24] T. Shindo *et al.*, "Lasing operation of lateral-current-injection membrane DFB laser with surface grating," in *Proc. 16th Opto-Electron. Commun. Conf.*, Kaohsiung, Taiwan, pp. 287–288, Jul. 2011, Paper 6D3_7.

[25] M. Futami *et al.*, "Low-threshold operation of LCI-membrane-DFB lasers with Be-doped GaInAs contact layer," in *Proc. 24th Int. Conf. Indium Phosphide Related Mater.*, Santa Barbara, CA, USA, pp. 285–288, Aug. 2012, Paper Th-2C.5.

[26] K. Doi *et al.*, "Room-temperature continuous-wave operation of lateral current injection membrane laser," in *Proc. 25th Int. Conf. Indium Phosphide Related Mater.*, Kobe, Japan, pp. 1–2, May 2013, Paper Wed2-3.

[27] D. Inoue *et al.*, "GaInAsP/InP lateral-current-injection membrane DFB laser integrated with GaInAsP waveguide on Si substrate," in *Proc. Int. Semicond. Laser Conf.*, Palma de Mallorca, Spain, pp. 32–33, Sep. 2014, Paper MB.03.

[28] S. Matsuo *et al.*, "Ultralow operating energy of directly modulated DFB laser on SiO_2/Si substrate,"presented at the Eur. Conf. Opt. Commun., Cannes, France, Sep. 2014, Paper Mo.4.4.3.

[29] T. Shindo *et al.*, "Design of lateral-current-injection-type membrane distributed-feedback lasers for on-chip optical interconnection," *IEEE J. Sel. Topics Quantum Electron.*, vol. 19, no. 4, art. no. 1502009, Jul./Aug. 2013.

[30] K. Kudo, J. I. Shim, K. Komori, and S. Arai, "Reduction of effective linewidth enhancement factor $\alpha_{\rm ex}$ of DFB lasers with complex coupling coefficients," *IEEE Photon. Technol. Lett.*, vol. 4, no. 6, pp. 531–534, Jun. 1992.

[31] H. Kogelnik and C. V. Shank, "Coupled-wave theory of distributed feedback lasers," *J. Appl. Phys.*, vol. 43, no. 5, pp. 2327–2335, May 1972.

[32] G. Björk and O. Nelsson, "A new exact and efficient numerical matrix theory of complicated laser structures: Properties of asymmetric phaseshifted DFB lasers," *J. Lightw. Technol.*, vol. LT-5, pp. 140–146, Jan. 1987.

[33] M. Asada and Y. Suematsu, "The effects of loss and nonradiative recombination on the temperature dependence of threshold current in 1.5–1.6 μm GaInAsP/InP lasers," *IEEE J. Quantum Electron.*, vol. QE-19, no. 6, pp. 917–922, Jun. 1983.

[34] L. A. Coldren and S. W. Corzine, *Diode Lasers and Photonic Integrated Circuits*, 1st ed. New York, NY, USA: Wiley-Interscience, 1995.

[35] K. Doi *et al.*, "Thermal analysis of lateral-current-injection membrane distributed feedback laser," *IEEE J. Quantum Electron.*, vol. 50, no. 5, pp. 321–326, May 2014.

[36] J. Lee *et al.*, "Low-loss GaInAsP wire waveguide on Si substrate with benzocyclobutene adhesive wafer bonding for membrane photonic circuits," *Jpn. J. Appl. Phys.*, vol. 51, no. 4, pp. 042201–1–042201-5, Mar. 2012.

[37] M. J. R. Heck and J. E. Bowers, "Energy efficient and energy proportional optical interconnects for multi-core processors: driving the need for on-chip sources," *IEEE J. Sel. Topics Quantum Electron.*, vol. 20, no. 4, art. no. 8201012, Jul./Aug. 2014.

[38] K. Ohira, T. Murayama, S. Tamura, and S. Arai, "Low-threshold and high efficiency operation of distributed reflector lasers with width-modulated wirelike active region," *IEEE J. Sel. Topics Quantum Electron.*, vol. 11, no. 5, pp. 1162–1168, Sep./Oct. 2013.

[39] T. Shindo *et al.*, "Low-threshold and high-efficiency operation of distributed reflector laser with wirelike active regions," *IEEE Photon. Technol. Lett.*, vol. 21, no. 19, pp. 1414–1416, Oct. 2009.

[40] D. Takahashi *et al.*, "Carrier-transport-limited modulation bandwidth in distributed reflector lasers with wirelike active regions," *IEEE J. Quantum Electron.*, vol. 48, no. 5, pp. 688–695, May 2012.

[41] T. Okumura, T. Koguchi, H. Ito, N. Nishiyama, and S. Arai, "Injection-type GaInAsP/InP membrane buried heterostructure distributed feedback laser with wirelike active regions," *Appl. Phys. Exp.*, vol. 4, no. 4, pp. 042101-1–042101-3, Apr. 2011.

[42] D. Inoue *et al.*, "Room-temperature continuous-wave operation of GaInAsP/InP lateral-current-injection membrane laser bonded on Si substrate," *Appl. Phys. Exp.*, vol. 7, pp. 072701-1–072701-4, Jul. 2014.

[43] M. Fujita, A. Sakaki, and T. Baba, "Ultrasmall and ultralow threshold GaInAsP-InP microdisk injection lasers: Design, fabrication, lasing characteristics, and spontaneous emission factor," *IEEE J. Sel. Topics Quantum Electron.*, vol. 5, no. 3, pp. 673–681, May/Jun. 1999.

[44] R. S. Tucker, J. M. Wiesenfeld, P. M. Downey, and J. E. Bowers, "Propagation delays and transition times in pulse modulated semiconductor lasers," *Appl. Phys. Lett.*, vol. 48, pp. 1707–1709, Apr. 1986.

[45] M. Sotoodeh, A. H. Khalid, and A. A. Rezazadeh, "Empirical low-field mobility model for III-V compounds applicable in device simulation codes," *J. Appl. Phys.*, vol. 87, no. 6, pp. 2890–2900, Mar. 2000.

[46] A. Katz *et al.*, "Pt/Ti/p In0.53Ga0.47As low-resistance nonalloyed ohmic contact formed by rapid thermal processing," *Appl. Phys. Lett.*, vol. 54, pp. 2306–2308, Mar. 1989.

[47] G. Franz and M.-C. Amann, "Extremely low contact resistivity of Ti/Pt/Au contacts on p^+ - InGaAs as determined by a new evaluation method," *J. Electrochem. Soc.*, vol. 140, no. 3, pp. 847–850, Mar. 1993.

[48] H. C. Casey, Jr., and P. L. Carter, "Variation of intervalence band absorption with hole concentration in p-type InP," *Appl. Phys. Lett.*, vol. 44, pp. 82–83, 1984.

[49] N. Nishiyama, C. Caneau, J. D. Downie, M. Sauer and C.-E. Zah, "10-Gbps 1.3 and 1.55-μm InP-based VCSELs: 85°C 10-km error-free transmission and room temperature 40-km transmission at 1.55-μm with EDC," presented at the Opt. Fiber Commun. Conf., 2006, Paper PDP23.

[50] G. P. Agrawal, *Fiber-Optic Communication Systems*. New York, USA: Wiley, 2010.

Takuo Hiratani (S'13) was born in Ishikawa, Japan, in 1990. He received the B.E. degree in electrical and electronic engineering from Kanazawa University, Ishikawa, Japan, in 2012 and the M.E. degree in electrical and electronic engineering from the Tokyo Institute of Technology, Tokyo, Japan, in 2014, where he is currently working toward the Ph.D. degree in electrical and electronic engineering.

His current research interests include membrane-based photonic devices for optical interconnection.

Mr. Hiratani is a Student Member of the Institute of Electronics, Information and Communication Engineers and the Japan Society of Applied Physics.

Takahiko Shindo (S'10–M'12) received the B.E., M.E., and Ph.D. degrees in electrical and electronic engineering from the Tokyo Institute of Technology, Tokyo, Japan, in 2008, 2010, and 2012, respectively.

After receiving the Ph.D. degree in 2012, he focused on semiconductor lasers with an ultralow-power-consumption operation, working as a Research Fellow at the Japan Society for the Promotion of Science, Japan. He joined NTT Photonics Laboratories in April 2013.

Dr. Shindo is a Member of the Japan Society of Applied Physics. He received the Best Student Paper Award at the Opto-Electronics and Communications Conference, Taiwan, and the Ericsson Young Scientist Award in 2012.

Kyohei Doi was born in Saitama, Japan, in 1988. He received the B.E. and M.E. degrees in electrical and electronic engineering from the Tokyo Institute of Technology, Tokyo, Japan, in 2012 and 2014, respectively. His research interests include the development of membrane-based photonic devices for optical interconnection. He joined the Bank of Tokyo-Mitsubishi UFJ, Ltd., in 2014.

Mr. Doi is a Member of the Japan Society of Applied Physics.

Yuki Atsuji was born in Tokyo, Japan, in 1991. He received the B.E. degree from University of Electro-Communications, Tokyo, Japan, in 2013, and he is currently working toward the M.E. degree in the Department of Electrical and Electronic Engineering, Tokyo Institute of Technology, Tokyo.

His current research interests include membrane-based photonic devices for optical interconnection.

Daisuke Inoue was born in Okayama, Japan, in 1990. He received the B.E. degree in electrical and electronic engineering from the Tokyo Institute of Technology, Tokyo, Japan, in 2013, where he is currently working toward the M.E. degree in electrical and electronic engineering.

His current research interests include membrane-based photonic devices for optical interconnection.

Mr. Inoue is a Student Member of the Institute of Electronics, Information and Communication Engineers and the Japan Society of Applied Physics.

Tomohiro Amemiya (S'06–M'09) received the B.S. and Ph.D. degrees in electronic engineering from the University of Tokyo, Tokyo, Japan, in 2004 and 2009, respectively.

In 2009, he moved to the Quantum Electronics Research Center, Tokyo Institute of Technology, where he is currently an Assistant Professor.

His research interests include physics of semiconductor light-controlling devices, metamaterials for optical frequencies, magnetooptical devices and the technologies for fabricating these devices.

Dr. Amemiya is a Member of the Optical Society of America, the American Physical Society, and the Japan Society of Applied Physics. He received the 2007 IEEE Photonics Society Annual Student Paper Award, the 2008 IEEE Photonics Society Graduate Student Fellowship, and the 2012 Konica Minolta Imaging Award.

Nobuhiko Nishiyama (M'01–SM'07) was born in Yamaguchi, Japan, in 1974. He received the B.E., M.E., and Ph.D. degrees from the Tokyo Institute of Technology, Tokyo, Japan, in 1997, 1999, and 2001, respectively.

During his Ph.D. work, he demonstrated single-mode 0.98- and 1.1-μm VCSEL arrays with stable polarization using misoriented substrates for high-speed optical networks as well as MOCVD-grown GaInNAs VCSELs. He joined Corning, Inc., New York, NY, USA, in 2001 and worked with the Semiconductor Technology Research Group. At Corning, he worked on several subjects, including short-wavelength lasers, 1060-nm DFB/DBR lasers, and long-wavelength InP-based VCSELs. Since 2006, he has been an Associate Professor with the Tokyo Institute of Technology. His current main interests include transistor lasers, silicon photonics, III–V silicon hybrid optical devices, and terahertz–optical signal conversions involving optics–electronics–radio integration circuits.

Dr. Nishiyama is a Member of the Japan Society of Applied Physics, IEICE, and IEEE Photonics Society. He received the Excellent Paper Award from the Institute of Electronics, Information and Communication Engineers (IEICE) of Japan in 2001 and the Young Scientists Prize in the Commendation for Science and Technology from the Minister of Education, Culture, Sports, Science, and Technology in 2009.

Shigehisa Arai (M'83–SM'06–F'10) was born in Kanagawa, Japan, in 1953. He received the B.E., M.E., and D.E. degrees in electronics from Tokyo Institute of Technology, Tokyo, Japan, in 1977, 1979, and 1982, respectively. During his Ph.D. work, he demonstrated room-temperature CW operations of 1.11–1.67 μm long-wavelength lasers fabricated by liquid-phase epitaxy as well as their single-mode operations under rapid direct modulation.

He joined the Department of Physical Electronics, Tokyo Institute of Technology, as a Research Associate in 1982, and joined AT&T Bell Laboratories, Holmdel, NJ, USA, as a Visiting Researcher from 1983 to 1984, on leave from the Tokyo Institute of Technology. Further, he became a Lecturer in 1984, an Associate Professor in 1987, and a Professor with the Research Center for Quantum Effect Electronics and the Department of Electrical and Electronic Engineering in 1994. Since 2004, he has been a Professor with the Quantum Nanoelectronics Research Center, Tokyo Institute of Technology. His research interests include photonic integrated devices such as dynamic-single-mode and wavelength-tunable semiconductor lasers, semiconductor optical amplifiers, and optical switches/modulators. His current research interests include studies of low-damage and cost-effective processing technologies of ultrafine structures for high-performance lasers and photonic integrated circuits on silicon platforms.

Dr. Arai is a Member of the Optical Society of America, the Institute of Electronics, Information and Communication Engineers (IEICE), and the Japan Society of Applied Physics (JSAP). He received the Excellent Paper Award from the IEICE of Japan in 1988, the Michael Lunn Memorial Award from the Indium Phosphide and Related Materials Conference in 2000, Prizes for Science and Technology including a Commendation for Science and Technology from the Minister of Education, Culture, Sports, Science and Technology in 2008, an Electronics Society Award and the Achievement Award from IEICE in 2008 and 2011, respectively, and a JSAP Fellowship in 2008.